NONIDEAL EFFECTS BEHIND REFLECTED SHOCK WAVES IN A HIGH-PRESSURE SHOCK TUBE

ERIC L. PETERSEN

The Aerospace Corporation
Mechanics and Propulsion Department
Los Angeles, CA

and

RONALD K. HANSON

Thermosciences Division
Department of Mechanical Engineering
Stanford University, Stanford, CA

1999 Technical Meeting
Joint Meeting of the United States Sections:
The Combustion Institute

The George Washington University
Washington, DC
March 15-17, 1999

Corresponding Author:

Eric Petersen
The Aerospace Corporation
M5-753
P.O Box 92957
Los Angeles, CA 90009-2957
Phone: (310) 336-2501
Fax: (310) 336-7680
e-mail: Eric.L.Petersen@aero.org

REPORT DOCUMENTATION PAGE

Form Approved
OMB NO. 0704-0188

1. AGENCY USE ONLY *(Leave blank)*

2. REPORT DATE
February 10, 2000

3. REPORT TYPE AND DATES COVERED
Technical Report

4. TITLE AND SUBTITLE
Nonideal Effects Behind Reflected Shock Waves in a High-Pressure Shock Tube

5. FUNDING NUMBERS
DAAG55-97-1-0300

6. AUTHOR(S)
E. L. Petersen[1] and R. K. Hanson[2]

7. PERFORMING ORGANIZATION NAME(S) AND ADDRESS(ES)
(1) The Aerospace Corporation,
Mechanics and Propulsion Department, Los Angeles, CA

(2) Stanford University
Department of Mechanical Engineering

8. PERFORMING ORGANIZATION REPORT NUMBER

9. SPONSORING / MONITORING AGENCY NAME(S) AND ADDRESS(ES)
U.S. Army Research Office
P.O. Box 12211
Research Triangle Park, NC 27709-2211

10. SPONSORING / MONITORING AGENCY REPORT NUMBER
ARO 36750.12-EG

11. SUPPLEMENTARY NOTES
The views, opinions and/or findings contained in this report are those of the author(s) and should not be considered as an official Department of the Army position, policy or decision, unless so designated by other documentation.

12a. DISTRIBUTION / AVAILABILITY STATEMENT
Approved for public release; distribution unlimited

12 b. DISTRIBUTION CODE

13. ABSTRACT *(Maximum 200 words)*

Shock tubes often experience temperature and pressure nonuniformities behind the reflected shock wave that cannot be neglected in chemical kinetics experiments. Because of increased viscous effects, smaller tube diameters, and nonideal shock formation, the reflected-shock nonidealities tend to be greater in higher-pressure shock tubes. Since the increase in test temperature (ΔT_5) is the most significant parameter for chemical kinetics, experiments were performed in the Stanford High Pressure Shock Tube using infrared emission from a known amount of CO in Argon. From the measured change in vibrationally equilibrated CO emission with time, the corresponding dT_5/dt (or $\Delta T5$ for a known time interval) of the mixture was inferred assuming an isentropic relationship between post-shock temperature and pressure changes. For a range of representative conditions in Argon (20-530 Atm, 1240-1900 K), the test temperature 2 cm from the endwall increased 3-8 K after 100 µs and 15-40 K after 500 µs, depending on the initial conditions. Separate pressure measurements using a shielded piezoelectric transducer confirmed the isentropic assumption. An analytical model of the reflected-shock gas dynamics was also developed. The measured incident-shock axial velocity profile and a model of the boundary layer growth provide the upstream boundary conditions needed to define the properties behind the moving reflected shock. The calculated ΔT_5's agree well with those obtained from experiment. The analytical model was used to estimate the effects of temperature and pressure nonuniformities on typical chemical kinetics measurements. When the kinetics are fast and occur in less than 300 µs, the temperature increase is typically negligible, although some correction is suggested for kinetics experiments lasting longer than 500 µs. The temperature increase, however, has a negligible impact on the measured absorption profiles of OH and CH_3 when using laser absorption diagnostics at 306 and 216 nm, respectively, validating the use of a constant absorption coefficient. Infrared emission experiments are more sensitive to temperature and pressure changes, so T_5 nonuniformities should be taken into account when interpreting IR-emission data.

14. SUBJECT TERMS

15. NUMBER OF PAGES

16. PRICE CODE

17. SECURITY CLASSIFICATION OF REPORT
UNCLASSIFIED

18. SECURITY CLASSIFICATION OF THIS PAGE
UNCLASSIFIED

19. SECURITY CLASSIFICATION OF ABSTRACT
UNCLASSIFIED

20. LIMITATION OF ABSTRACT
UL

NONIDEAL EFFECTS BEHIND REFLECTED SHOCK WAVES IN A HIGH-PRESSURE SHOCK TUBE

Eric L. Petersen[†] and Ronald K. Hanson

Abstract

Shock tubes often experience temperature and pressure nonuniformities behind the reflected shock wave that cannot be neglected in chemical kinetics experiments. Because of increased viscous effects, smaller tube diameters, and nonideal shock formation, the reflected-shock nonidealities tend to be greater in higher-pressure shock tubes. Since the increase in test temperature (ΔT_5) is the most significant parameter for chemical kinetics, experiments were performed to characterize ΔT_5 in the Stanford High Pressure Shock Tube using infrared emission from a known amount of CO in argon. From the measured change in vibrationally equilibrated CO emission with time, the corresponding dT_5/dt (or ΔT_5 for a known time interval) of the mixture was inferred assuming an isentropic relationship between post-shock temperature and pressure changes. For a range of representative conditions in argon (20–530 atm, 1240–1900 K), the test temperature 2 cm from the endwall increased 3–8 K after 100 μs and 15–40 K after 500 μs, depending on the initial conditions. Separate pressure measurements using a shielded piezoelectric transducer confirmed the isentropic assumption. An analytical model of the reflected-shock gas dynamics was also developed. The measured incident-shock axial velocity profile and a model of the boundary layer growth provide the upstream boundary conditions needed to define the properties behind the moving reflected shock. The calculated ΔT_5's agree well with those obtained from experiment. The analytical model was used to estimate the effects of temperature and pressure nonuniformities on typical chemical kinetics measurements. When the kinetics are fast and occur in less than 300 μs, the temperature increase is typically negligible, although some correction is suggested for kinetics experiments lasting longer than 500 μs. The temperature increase, however, has a negligible impact on the measured absorption profiles of OH and CH_3 when using laser absorption diagnostics at 306 and 216 nm, respectively, validating the use of a constant absorption coefficient. Infrared emission experiments are more sensitive to temperature and density changes, so T_5 nonuniformities should be taken into account when interpreting IR-emission data.

Introduction

Ideally, the temperature and pressure in the region behind reflected shock waves do not vary with time and are equal to the values calculated using classical theory. However, nonideal fluid mechanics such as incident-shock attenuation and boundary layer growth lead to temperatures and pressures behind the reflected shock wave that increase with time. Unfortunately, when performing chemistry measurements in a shock tube, errors in the reaction temperature can lead to large uncertainties in the rate coefficient or ignition delay time [1]. For example, the high-pressure rate coefficient of NO_2 has an activation energy of 300 kJ/mol (i.e., $k_\infty(T) = 4\times10^{14}\exp(300/RT)$) [2]. For an average temperature of 1500 K, a 15-K error in temperature (i.e., only 1%) can lead to a 25% uncertainty in the measured rate coefficient. Therefore, great care must be taken to minimize uncertainties in the shock tube test temperature, and many experimental and analytical studies were conducted by previous investigators to characterize shock tube temperature nonuniformities and determine their impact on measurement accuracy.

Most temperature and density corrections for incident-shock chemistry measurements have been based on the area-reduction equations of Mirels [3,4], which are simplified forms of

---

[†] When most of this work was performed, both authors were with Stanford University.

the more extensive boundary layer routines developed in earlier papers by Mirels. Some examples of incident-shock nonuniformity studies include those of Warshay [5], Belford and Strehlow [6], Belles and Brabbs [7,8], Bertin et al. [9], Fujii et al. [10], and Koshi and Asaba [11]. In general, boundary layer effects behind the incident shock wave are more important for longer test times, and incident-shock measurements are further complicated by the particle-time correction. Performing measurements behind the reflected shock wave where the flow is (ideally) stagnant eliminates many of the time-dependent problems with incident-shock measurements.

Early reflected-shock studies, however, uncovered large errors in T_5 which could seriously impact reflected-shock chemistry measurements [12-15]. Strehlow and Cohen [12] and Skinner [13] attributed the uncertainties to shock-wave/boundary-layer interaction in other than monatomic gases. Underpredictions between 30 and 200 K were estimated, and Brabbs et al. [14] observed significant reflected-shock temperature uncertainties even in argon. Strehlow and Case [15] in a later study found that temperatures in argon were overpredicted instead of underpredicted, while Johnson and Britton [16] claimed their Br decomposition measurements behind reflected shocks in an argon bath disagreed with similar data taken behind incident shock waves. Nitrous oxide decomposition measurements by Fishburne et al. [17] likewise displayed a discrepancy between rates obtained behind reflected waves versus those measured behind incident waves. Fortunately, later studies implicated errors in incident-shock velocity measurement, vibrational relaxation, test section location, etc. for the larger, unknown errors in reflected-shock temperature [1]. Optical measurements of the temperature support the values of T_5 calculated from ideal theory, assuming the shock tube diameter is large enough to minimize attenuation affects, and the bifurcation structure in di- and polyatomic test gases is minor [1,18].

Although the initial endwall T_5 is now routinely inferred from the incident-shock velocity, property variations behind the reflected shock wave due to incident-shock velocity attenuation and nonuniform incident-flow-field effects persist and must still be accounted for in certain cases. The test temperature and pressure vary because the reflected shock wave propagates into a gas that was processed by an attenuating incident shock wave with a boundary layer behind it. The perturbations in the nonuniform flow field upstream of the reflected shock lead to disturbance waves behind the reflected shock which influence the thermodynamic properties therein.

The present paper is concerned with nonideal conditions behind reflected shock waves in the Stanford High Pressure Shock Tube (HPST). Specifically, the temperature and pressure increase behind reflected shock waves in the HPST is characterized, and an analytical model that predicts the temperature rise behind the reflected shock wave for a given incident-shock velocity profile is presented. Finally, the effect of nonuniform temperature on typical reflected-shock chemical kinetics measurements in the HPST is presented in the form of high-pressure species-profile calculations and measurements.

Shock Tube and Attenuation

The Stanford HPST, described in more detail by Petersen [19], has a 3-m, 7.62-cm-dia driver and a 5-m, 5-cm-dia driven section. For most experiments, the driver gas is helium, and the test gas is predominantly argon. The shock tube uses steel or aluminum diaphragms in either a single- or double-diaphragm mode of operation. As mentioned above, a common indication of shock tube nonidealty is the attenuation of the incident shock wave. On the HPST, the incident-shock velocity as a function of axial distance is measured via six fast-response piezoelectric pressure transducers (PCB 113A) and five Phillips PM6666 time-interval counters over roughly the last meter before the endwall. Typical shock attenuations, defined as the normalized slope of axial velocity as extrapolated to the endwall (in %/meter), range from 1 to 4%. The incident-shock attenuation in the HPST is due primarily to boundary layer layer buildup [3,4,19] and nonideal rupture of the diaphragm(s) [19].

Ideally, diaphragm breakage and shock formation occur instantaneously, but measurements by previous investigators indicate the diaphragm opening process can take hundreds of microseconds [20]. The finite opening time of the diaphragm can affect the shock formation distance and trajectory [21-27] and, in general, slow-opening diaphragms cause the peak in axial shock trajectory to occur further downstream [22]. The resulting slope of the attenuating shock downstream of the peak Mach number can be steeper than predicted assuming viscous effects alone [23]. Opening time/formation distance has been found to vary inversely with driver-to-driven pressure difference, P_{41} (i.e, P_4-P_1), and directly with diaphragm density, diaphragm thickness, ultimate stress of the diaphragm material, and shock tube diameter [24]. For the HPST, the shock formation distance and diaphragm opening time are not routinely measured, but these cited trends qualitatively support the observed test-to-test variation in the incident-shock attenuation. Variations in the scribe depth (i.e., diaphragm thickness), total diaphragm material volume, and rate of P_4-filling (i.e, rate of stress on the diaphragm) for single-diaphragm experiments were found to contribute to deviations in the measured shock trajectory.

A representative range of attenuation data are presented as a function of incident-shock Mach number at the endwall (M_s) and fill pressure (P_1) in Fig. 1. If the attenuation were due solely to the viscous boundary layer, the attenuation would vary with Mach number and fill pressure per

$$\text{Attenuation}(\% / \text{m}) \propto P_1^{-0.14}\sqrt{M_s} \tag{1}$$

and follow the calculated attenuation curve. Equation 1 was derived using the analytical shock tube boundary layer models presented by Petersen [19] and Mirels [3,4]. However, the actual attenuation data are higher than the calculated values and exhibit large scatter (± 0.5%/m). The large scatter and higher attenuation indicate nonideal effects other than viscosity, such as nonideal diaphragm breakage and test-to-test variations in diaphragm thickness, contribute to the overall attenuation. From the results of Fig. 1, one can conclude that wall viscous effects comprise approximately 70% (or more) of the total shock attenuation, while nonideal shock formation contributes the remaining 30% (or less). Nonetheless, the total attenuation varies roughly with M_s and P_1 as predicted by attenuation theory. The steel diaphragms tend to produce lower attenuation than the aluminum diaphragms primarily because of the higher fill pressures involved, per Eqn. 1 (note that higher fill pressures correspond to higher test, or P_5, pressures).

Perhaps the most significant aspect of the Fig. 1 attenuation data is the relatively high degree of incident-shock attenuation when compared to the ≈1%/m attenuation typically observed in many low-pressure shock tubes. A significant contributor to the increased attenuation is the enhanced effect of viscosity due in part to the higher pressure and the smaller tube diameter. Since the test pressure is often 2 to 3 orders of magnitude higher than in lower pressure shock tubes, the Reynolds number is higher, leading to a situation where the boundary layer can be assumed turbulent immediately behind the incident shock wave. The turbulent boundary layer results in a much thicker boundary layer than would exist if the layer were laminar at the same pressure [19]. The effects of test pressure and diameter on the turbulent boundary layer and the resulting reflected-shock nonuniformity are detailed in the analytical-model calculations below.

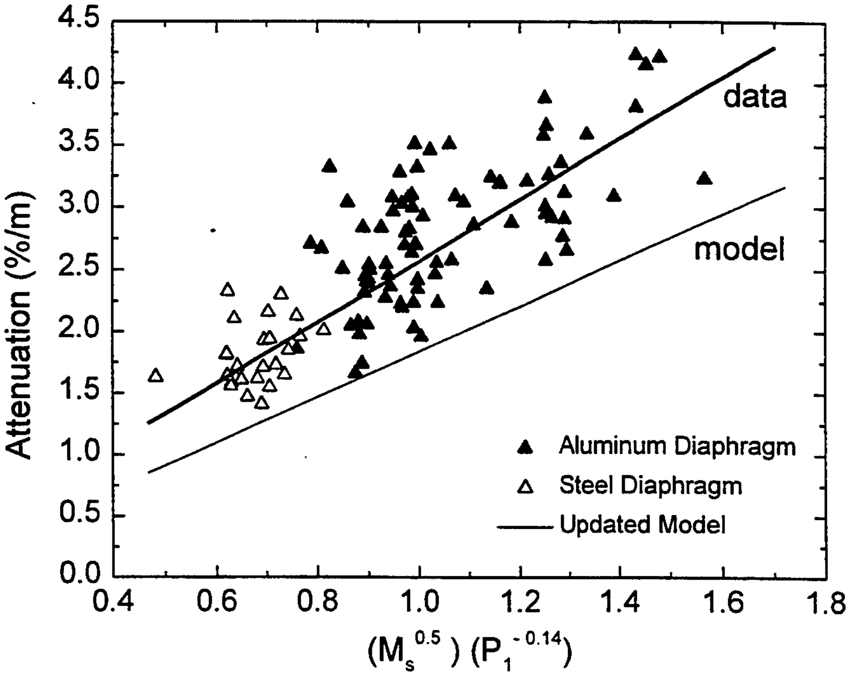

Fig. 1 Sample HPST incident-shock attenuation data in argon as a function of Mach number and fill pressure (in atm). The data are compared to the analytical shock-attenuation model of Petersen [19] and Mirels [3,4], which includes only viscous effects.

Temperature Measurements

Although many experimenters use analytical methods to predict and correct for nonideal affects due to boundary layer growth and shock attenuation, actual measurements of the temperature and pressure changes are preferred. Therefore, measurements of the temperature increase behind reflected shock waves were performed in the HPST over a range of elevated pressures and are summarized in this section.

Background

Others have utilized various optical methods to explore and characterize the shocked-gas temperature in low-pressure shock tubes. For example, line reversal techniques have been employed to measure very high temperatures [28-31]. More recently, a rapid-tuning ring-dye laser was used to measure the temperature behind incident [32] and reflected [33] shock waves by taking the ratio of the $R_1(7)$ and $R_1(11)$ OH lines of the A←X transition near 306.5 nm; the OH was generated in an argon bath seeded with a stoichiometric H_2-O_2 mixture. The quoted accuracy for the laser-based absorption technique was 3%, or 40-100 K for the temperature ranges considered.

An alternate method for obtaining the hot-gas temperature in a shock tube involves monitoring the infrared emission from vibrationally excited molecules, present in small quantities. Once this minor constituent is vibrationally equilibrated, its temperature approaches the bulk-gas temperature and, through calibration of the optical setup, the bulk-gas temperature can be determined. Lapworth et al. [34] and Guinee et al. [35] used the carbon monoxide and carbon dioxide vibrational bands near 4.7 μm, respectively, to measure the absolute reflected-shock temperature with a three-percent error.

A simpler method involves the measurement of ΔT only, so tedious calibration of the ir measurement apparatus is not needed (which, regardless, may not be accurate enough to discern temperature changes within 50 K). Just and Schmalz (CO) [36], Flower (CO) [37], Hayashi and Goto (CO_2) [38], and Ciezki and Adomeit (CO_2) [39] have used this ΔT method to characterize the temperature uniformity of post-shock gases in their respective facilities. In the present application, knowledge of the absolute temperature was not as important as measurement of the temperature increase, so an infrared emission technique was used to determine the temperature increase behind reflected shocks in the HPST. Details of the measurements and their results are described below.

Measurement Procedure

Experiments using the Fig. 2 infrared emission setup were conducted behind reflected shock waves in the HPST to characterize the temperature nonuniformity. Small fractions of CO (500-8000 ppm) were pre-mixed with the argon test gas; at elevated temperatures and pressures, the CO molecules became vibrationally excited and emitted infrared radiation that was detected by the ir-emission setup. A narrow-band filter ($\lambda = 4.181 - 4.742$ μm, FWHM) was employed to monitor only emission from the CO fundamental vibration centered near 2143 cm^{-1}. To accelerate the relatively slow vibrational relaxation of the CO molecules, small amounts of H_2 were added to the mixtures. All emission measurements were performed 20 mm from the shock tube endwall.

A 5-cm-diameter parabolic mirror with a 15-cm focal length was utilized in the optical setup (Fig. 2). The mirror was located 45 cm from the near inside wall of the shock tube, and the InSb detector (Judson J10D-DB3-1X3M-MTL) was placed 22 cm from the focusing mirror. The slit size was typically 1 mm and was positioned 17 cm from the inside wall of the shock tube, directly external to the retaining stud. A Delrin plug was used in the port directly opposite the sapphire window to minimize the background emission from the shock tube walls. The small, residual background emission (see Petersen [19]), although characterized for the conditions of the CO-emission tests [40], was not a factor in the relative temperature calculations; no correction to the signals was, needed. Similarly, the minor self-absorption observed in the highest CO-concentration mixtures [40] did not influence the ΔT measurements and was therefore ignored in the calculations.

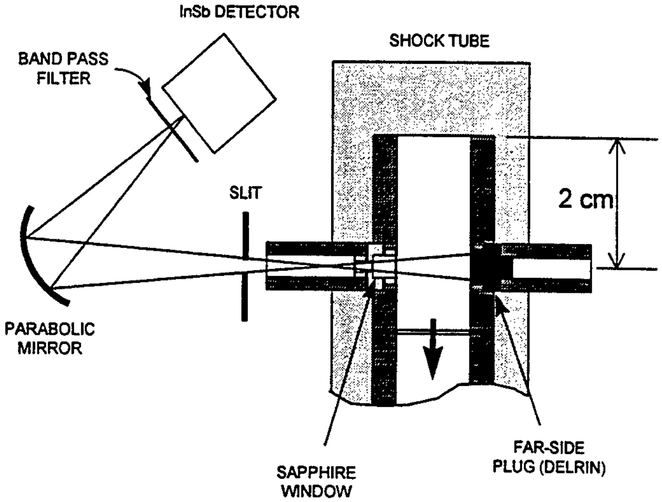

Fig. 2 Infrared emission setup for the Stanford High Pressure Shock Tube (not to scale)

Unshielded pressure measurements were also taken during the IR-emission experiments. However, while the pressure traces exhibited attenuation effects (i.e., an increasing pressure), the results were sensitive to heat transfer from the post-shock gases. As a result, pressure was not used to infer the density changes behind the reflected shock wave for the CO-emission tests herein. Details on the relationship between attenuation effects and the measured pressure are discussed in a later section.

The basis for the temperature measurements is the relationship between the measured ir-emission intensity and the temperature and density of the emitting molecules. Assuming the harmonic oscillator model for the CO vibration [41], the emission intensity is [36,38,39]

$$I = \frac{\beta[\mathrm{CO}]}{e^{\theta_v/T} - 1} = \frac{\beta}{e^{\theta_v/T} - 1}\left(\frac{P_{CO}}{R_u T}\right) \tag{2}$$

where β is the calibration constant of the optical setup, T is the temperature, P_{CO} is the partial pressure of CO, R_u is the universal gas constant, and $\theta_v = h\nu/k$. The θ_v constant for CO is equal to 3085 K for the average oscillation frequency, ν, of 2143 cm^{-1}. If the calibration constant β were known, Eqn. 2 could be solved for the absolute temperature for a given CO mole fraction, pressure, and emission intensity. However, since the change in temperature was the parameter of primary interest, Eqn. 2 was instead differentiated and normalized to the initial conditions. The initial temperature and pressure (T_o and P_o) were assumed to be the values calculated from the measured incident-shock velocity and the ideal, 1-D theory at the time immediately after shock reflection from the endwall.

Differentiating I(T,P) in Eqn. 2 with respect to time, normalizing by the initial values I_o, T_o, and P_o, and solving for dT/dt results in, for relatively small changes in P and T (i.e., $P \approx P_o$ and $T \approx T_o$)

$$\frac{d(T/T_o)}{dt} \cong \left[\frac{d(I/I_o)}{dt} - \frac{d(P/P_o)}{dt}\right] \frac{T_o\left(e^{\theta_v/T_o}-1\right)}{\left[e^{\theta_v/T_o}(\theta_v - T_o) + T_o\right]} \tag{3}$$

Assuming the relationship between the pressure and temperature is isentropic (i.e., adiabatic and reversible), the isentropic change in pressure can be shown to be

$$\left.\frac{dP}{dt}\right|_{isen} = \frac{P_o}{T_o}\left(\frac{\gamma}{\gamma-1}\right)\left(\frac{P}{P_o}\right)^{\frac{1}{\gamma}} \frac{dT}{dt} \tag{4}$$

Combining Eqns. 3 and 4, again invoking the approximation that $P/P_o \approx 1$, the final expression for the temperature slope as a function of the measured change in ir emission is

$$\frac{d(T/T_o)}{dt} \cong \frac{B\frac{d(I/I_o)}{dt}}{1 + B\frac{\gamma}{(\gamma-1)}} \tag{5}$$

where

$$B = \frac{T_o(e^{\theta_v/T_o}-1)}{\left[e^{\theta_v/T_o}(\theta_v - T_o) + T_o\right]} \tag{6}$$

By assuming an isentropic relationship between the temperature and pressure, the need for pressure measurements is alleviated. Previous investigators likewise assumed their reflected-shock flow fields were isentropic [36-39]. Both analytical-model predictions and shielded pressure measurements support the isentropic assumption (see below).

Carbon Monoxide Emission Measurements

A number of CO infrared emission measurements were performed (mostly in conjunction with other studies [40]) from which the increase in temperature behind the reflected shock wave was inferred. Presented in Table 1 are 76 representative experiments covering reflected-shock temperatures between 1240 and 1900 K and pressures from 20 to 530 atm. Since the percentages of CO and H_2 in the test gas were small (typically << 1%), and assuming the CO vibrationally equilibrated to the bath-gas temperature, the ΔT results herein pertain to a pure-argon driven gas.

A noticeable increase in IR emission at times after passage of the reflected shock wave was observed in each experiment. This trend is evident in the sample emission signal displayed in Fig. 3, normalized to its time-zero value. A common trend in all the experiments was the near-linear behavior of the increasing emission. Hence, the results listed in Table 1 assume constant slopes, normalized to I_o. From the measured dI/dt, the changes in pressure and temperature could be calculated via Eqns. 4 and 5, respectively. These dT/dt and dP/dt results (normalized to T_o and P_o) are also provided in Table 1.

Table 1 Reflected-shock nonuniformity data from CO-emission experiments. The slopes are normalized to their initial values. The * signifies the variable is normalized to its initial, time-zero value.

Run	T (K)	P (atm)	Att (%/m)	dI^*/dt (s^{-1})	dP^*/dt (s^{-1})	dT^*/dt (s^{-1})
862	1450	19.6	3.20	205.0	131	52
875	1275	61.1	3.50	144.0	87	35
884	1379	62.3	3.96	151.0	94	38
885	1641	59.2	4.12	173.0	116	47
887	1489	59.2	3.76	160.0	103	41
888	1783	52.8	3.72	201.0	108	43
890	1815	52.8	3.81	137.0	96	38
891	1522	60.4	3.99	132.0	86	34
892	1521	37.7	3.79	126.0	82	33
897	1335	33.4	2.89	143.0	88	35
907	1461	33.1	3.53	187.0	120	48
915	1424	32.1	4.01	171.0	108	43
916	1464	33.7	3.56	186.0	119	48
931	1410	62.9	2.93	125.0	79	32
932	1598	61.1	3.26	135.0	90	36
933	1493	33.6	3.01	144.0	93	37
934	1696	31.8	3.19	170.0	116	46
938	1546	24.8	3.32	154.0	101	40
1075	1431	67.7	3.39	100.2	64	25
1077	1509	61.7	4.06	119.1	77	31
1096	1611	196.7	2.52	85.0	57	23
1097	1586	63.7	3.08	101.2	67	27
1098	1622	199.1	1.93	110.9	74	30
1103	1628	198.8	2.09	109.2	73	29
1104	1460	205.3	1.72	99.4	64	25
1105	1624	166.4	2.32	92.9	62	25
1106	1439	181.3	1.91	86.4	55	22
1131	1445	176.7	1.82	99.2	63	25
1132	1499	173.8	2.18	88.2	57	23
1133	1528	161.4	1.97	81.1	53	21
1149	1803	158.7	2.16	135.2	94	38
1150	1722	159.8	2.14	113.0	77	31
1151	1711	160.8	2.24	114.2	78	31
1174	1452	69.2	2.59	109.5	70	28
1175	1470	70.5	3.02	98.9	64	25
1182	1485	70.7	3.25	94.2	61	24
1183	1642	66.8	2.66	99.7	67	27
1184	1895	63.3	3.35	126.3	90	36
1185	1508	72.6	3.60	94.6	61	25
1187	1443	192.7	1.70	85.3	54	22
1190	1566	69.7	3.91	97.4	64	26
1191	1581	493.3	1.89	92.1	61	24
1193	1492	71.3	3.22	110.4	71	29
1194	1436	69.3	2.52	98.4	63	25
1197	1580	64.3	3.48	114.3	76	30
1198	1803	60.2	3.70	129.3	90	36
1201	1300	166.6	1.93	93.2	57	23
1204	1366	63.0	2.93	94.3	59	23
1206	1469	69.9	3.31	94.7	61	24
1207	1402	65.5	2.15	120.2	76	30
1211	1628	66.4	2.71	148.4	100	40
1214	1399	65.6	2.54	121.4	76	31
1216	1314	168.6	1.20	97.8	60	16
1217	1602	164.0	2.58	100.5	67	21
1218	1748	160.4	2.09	122.0	84	29
1219	1376	63.5	2.68	112.5	70	19
1221	1771	58.3	3.65	164.0	114	40
1222	1389	174.8	2.24	98.0	61	17
1223	1398	90.2	2.27	94.3	59	17
1224	1854	162.1	2.34	134.2	94	35
1226	1556	62.3	4.33	103.5	68	21
1228	1541	278.5	1.74	88.7	58	18
1229	1782	280.9	2.40	112.0	78	28
1235	1619	65.5	3.26	128.2	86	28
1236	1536	60.7	3.50	126.9	83	26
1237	1529	302.9	1.91	91.2	60	18
1238	1424	316.7	1.94	85.6	54	15
1239	1374	316.4	1.44	91.2	57	16
1240	1885	270.3	1.56	157.2	111	42
1244	1520	64.0	3.23	130.3	85	26
1245	1489	62.4	2.73	124.0	80	24
1247	1398	510.3	1.26	86.0	54	15
1248	1358	505.4	1.92	106.8	66	18
1250	1713	268.2	2.76	120.8	83	28
1251	1775	520.9	1.76	141.0	98	35
1252	1359	529.1	1.56	74.0	46	12

Possibly the most significant result of the temperature-characterization tests is that nonideal-flow effects cause the test temperature to increase with time. Typical ΔT's at 100 and 500 μs (inferred from the ir emission data) are given in Table 2 for a representative range of pressures and temperatures. The temperature rise at 100 μs can be as high as 8 K, and the temperature increase at 500 μs approaches 40 K or more. In general, the nonideal temperature effects are greatest at lower pressures (where the boundary layer is thicker and the incident-shock attenuation is higher) and higher temperatures. For pressures above 60 atm, the ΔT characteristics are similar.

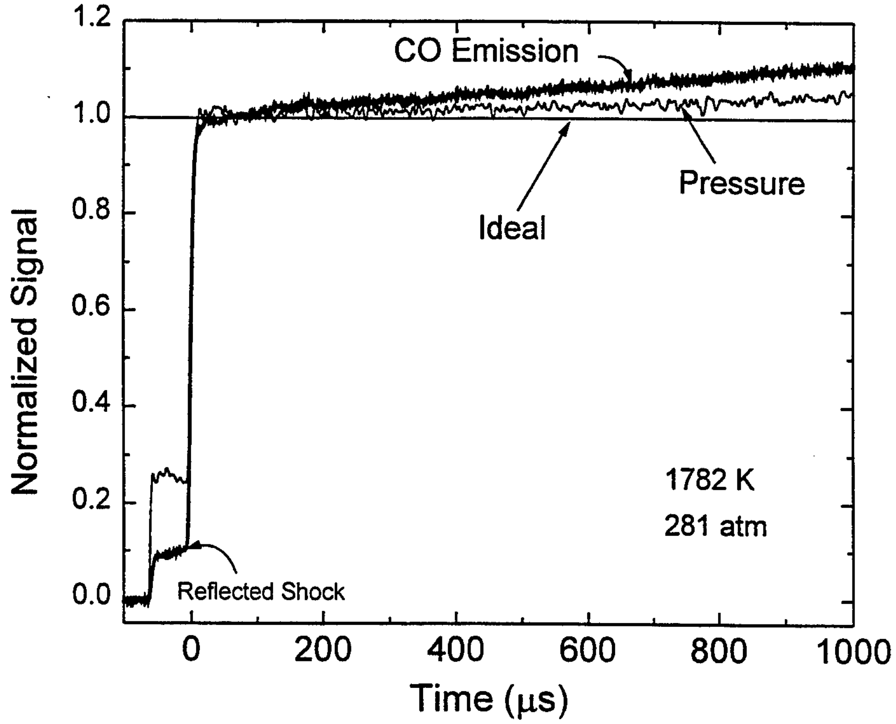

Fig. 3 Sample CO-emission and pressure measurements normalized to their time-zero values. The pressure measurement is from an unshielded PCB 113A transducer. 1782 K, 281 atm, 0.15% CO/0.85% H_2/99% Ar.

Table 2 Typical inferred temperature and pressure changes at 100 and 500 μs after reflected-shock passage.

			100 μs		500 μs	
Run	Po (atm)	To (K)	ΔP (atm)	ΔT (K)	ΔP (atm)	ΔT (K)
915	32.1	1424	0.4	6	1.7	31
934	31.8	1696	0.4	8	1.8	39
1174	69.2	1452	0.5	4	2.4	20
1184	63.3	1895	0.6	7	2.8	34
1222	174.8	1389	1.1	3	5.4	17
1224	162.1	1854	1.5	7	7.6	35
1239	316.4	1374	1.8	3	9.0	16
1240	270.3	1885	3	8	15.0	42
1248	505.4	1358	3.4	4	16.7	18
1251	520.9	1775	5.1	7	25.4	35

A primary side effect of the temperature increase is the potential for error in species-concentration and kinetics measurements behind the reflected shock wave. Species mole fractions derived from ir emission measurements must take into account the change in temperature and pressure with time, and the measurements should be adjusted accordingly. Similar temperature corrections must also be applied to data obtained from other techniques, particularly if the technique is a strong function of temperature. By combining the expected temperature increase with measured emission (or absorption) signals, better interpretation of kinetics data can be made.

While the measured temperature increase herein provides useful information on the nonidealities behind the reflected shock wave, CO-emission measurements are not (and cannot be) routinely performed on all experiments. Fortunately, the pressure can be used to infer changes in the test temperature by simply monitoring the change in pressure as a function of time. The resulting dT/dt can be inferred from Eqn. 5, assuming an isentropic relationship between T and P in addition to $P/P_0 \approx 1$. Such a method is convenient since the pressure is monitored on a routine basis, while temperature-measuring techniques such as CO emission cannot be employed on every shock tube experiment. A fast-response pressure transducer, shielded against heat transfer effects, was proven to be a reliable indication of the reflected-shock nonuniformities [19].

Figure 4 compares actual dP/dt measurements from a shielded pressure transducer to the isentropic assumption, where the agreement is satisfactory. Note that there is considerably more scatter when an unshielded transducer is utilized. The dT/dt values plotted on the horizontal axis were obtained from the reflected-shock analytical model, discussed in the following section, for the measured incident-shock attenuations. Calculated dT/dt values are used in Fig. 4 in lieu of measured values because the shielded transducer was, unfortunately, not employed for most of the CO-emission ΔT_5 experiments, as mentioned above; it is shown below that the reflected-shock model agrees well with available dT/dt measurements and can therefore be used in Fig. 4 without appreciable error.

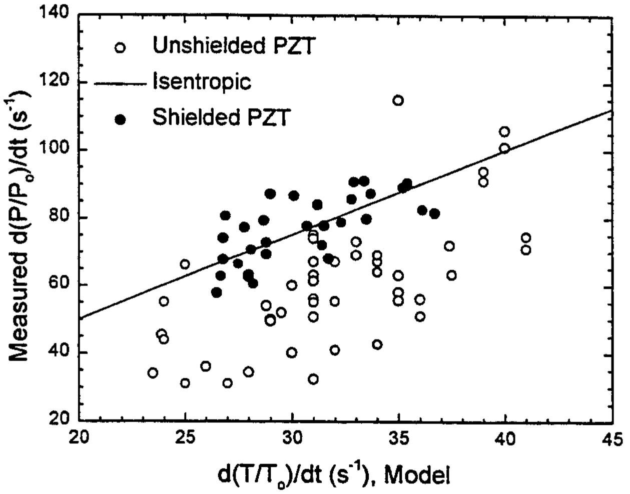

Fig. 4 Measured pressure rise behind reflected shock waves for an unshielded and a shielded pressure transducer. The dT/dt's were calculated with the reflected-shock analytical model.

Reflected-Shock Model

To supplement the experimental characterization and to gain insight into the physics of the nonideal effects, an analytical model was developed. Previous reflected-shock models are reviewed to provide a background into existing theory, followed by a presentation of the theory employed in the present model. Typical results from the theoretical model are then summarized and compared with measurement.

Background

While predictive models of nonideal behavior behind incident shock waves exist and have been employed to correct chemical kinetics measurements [5-11], comparatively few models are available to calculate nonideal behavior behind the reflected shock wave. Among the first theoretical works to address the reflected-shock/boundary layer interaction and its repercussions on conditions within the reflected region was that of Rudinger [43]. In his study, Rudinger assumed isentropic flow within the reflected- and incident-shock regions and used the theory of Mirels to predict the nonuniform conditions behind the incident shock wave. It was observed that relatively small pressure perturbations behind the incident shock wave are amplified into larger pressure increases behind the reflected shock. In later studies, Hanson [43,44] assumed small perturbations to predict nonuniformities behind the reflected shock caused by the propagation of the reflected wave into a nonuniform flow field. The nonuniform flow behind the incident wave was defined by a known incident-shock axial Mach number profile, and the simplified theory agreed well with a more-extensive, method of characteristics model.

One of the only theoretical works to address the effect of reflected-shock nonuniformities on chemical kinetic measurements is that of Michael and Sutherland [45]. In their paper, theory was compared to pressure and velocity measurements to develop a method for correcting the measured kinetics data for temperature and pressure perturbations, assuming isentropic flow within the reflected-shock region. Kinetics measurements in reflected shock waves at low Mach numbers using the correction method of Michael and Sutherland were presented in a later study [46]. The boundary-layer corrections led to lower rate coefficients and higher activation energies than those determined from ideal shock tube theory.

Theory

A reflected shock wave model was developed to estimate the nonuniformities attributed to the nonideal effects discussed above. The conditions into which the reflected shock wave travels are determined using the turbulent boundary layer and attenuation procedures presented by Mirels and [3,4] Petersen [19]. In general, the reflected-shock model is similar to the one used by Rudinger for a low-pressure shock tube, the primary exceptions being the improved turbulent friction model [19] and the use of measured/defined incident-shock velocity profiles as in Hanson [43,44]. By prescribing the shock trajectory in addition to the incident-flow nonuniformity, the nonideal effects due to both friction and diaphragm breakage are accounted for. The resulting effects on the conditions in the reflected-shock region at the measurement location are calculated using the techniques laid out in Rudinger [47]. The basic theory and model development are as follows.

A schematic diagram of the reflected-shock process is given in Fig. 5. Point A represents the measurement/test location in the shock tube. The lines CA and FD represent right-running characteristic waves, and DA a left-running wave, through which information in the form of pressure waves travels from the endwall and the region immediately behind the reflected shock wave to the test section. Therefore, disturbances due to nonuniform conditions upstream of the reflected shock wave can influence the pressure and temperature at point A. Lines CA and FD are defined as P-waves, and line DA represents a Q-wave.

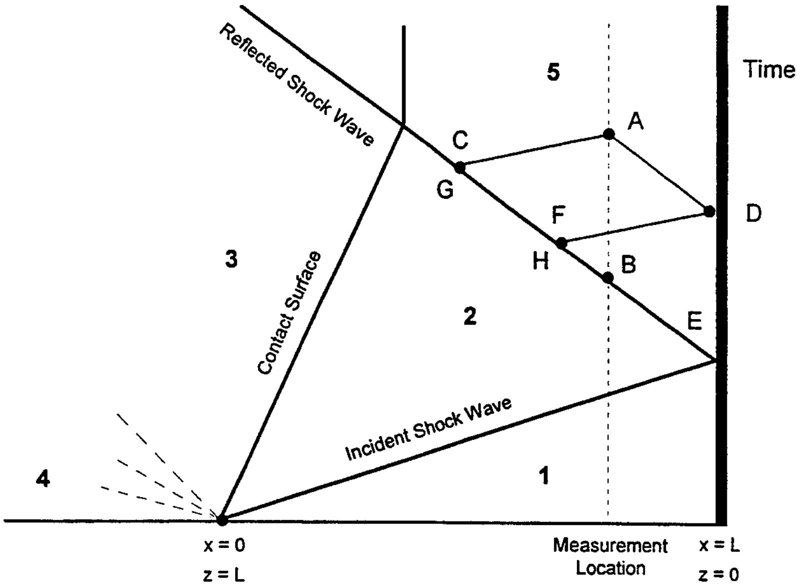

Fig. 5 x-t diagram for reflected shock wave.

As discussed in Rudinger [47], it is convenient to define the Riemann variables for the P and Q waves as

$$P = \frac{2}{(\gamma - 1)} a + u \tag{7}$$

$$Q = \frac{2}{(\gamma - 1)} a - u \tag{8}$$

where γ is the specific heat ratio, a is the sound speed $(\gamma RT)^{1/2}$, and u is the bulk fluid velocity in the x direction. Upon solution of the continuity and momentum equations, it can be shown that the P and Q characteristic waves are related to the entropy via

$$\frac{\partial P}{\partial t} + (a + u)\frac{\partial P}{\partial x} = a\left[\gamma \frac{\partial S}{\partial t} + (a + \gamma u)\frac{\partial S}{\partial x}\right] \tag{9}$$

$$\frac{\partial Q}{\partial t} + (a-u)\frac{\partial Q}{\partial x} = a\left[\gamma\frac{\partial S}{\partial t} + (a-\gamma u)\frac{\partial S}{\partial x}\right] \quad (10)$$

The normalized entropy, S, is defined relative to the initial conditions in region 1 as follows:

$$S = \frac{s - s_1}{c_p(\gamma - 1)} = \frac{1}{(\gamma - 1)}\ln(T/T_1) - \frac{1}{\gamma}\ln(P/P_1) \quad (11)$$

where s is the entropy, c_p is the constant-pressure specific heat and, of course, the P in Eqn. 11 is the pressure and not the Riemann variable.

Equations 7 through 11 are combined with the definition of the sound speed in a perfect gas to solve for the conditions at point A as a function of time, remembering that Eqns. 9 and 10 only apply along the waves defined in Fig. 5. In the solution procedure, the conditions at points C and F are obtained from the normal-shock relations while the conditions at points G and H, respectively, are calculated using the incident-shock/boundary layer techniques outlined in Petersen [19] and Mirels [3,4]. The conditions immediately downstream of the reflected shock wave are given relative to the upstream conditions by the classical 1-D normal shock relations [28]. The trajectory of the reflected shock wave must be provided. In the present model, the reflected-shock velocity w_R is assumed to be constant and equal to the lab-frame velocity defined at point E. (The conditions at point E are known from the measured incident-shock trajectory and the initial driven-gas conditions.)

A further assumption is that the flow is adiabatic, implying that each mass particle behaves isentropically. Since the flow within region 5 is virtually stagnant, the particle paths are nearly vertical lines on an x-t diagram. The entropy at point A, therefore, remains the same as that at point B (which is known). This multi-isentropic assumption and the assumption that the bulk flow velocity is negligible were confirmed in separate calculations. This greatly simplifies the solution of Equations 9 and 10, wherein the CA, DA, and FD characteristics lead to $P_A = P_C$, $Q_A = Q_D$, and $Q_D = P_D = P_F$ (since $u_D = 0$ from the wall boundary condition). Therefore, u_A, T_A, and T_D can be found by repeated application of the Riemann relations (Eqns. 7 and 8) and the speed of sound. Equation 11 is then used to obtain the pressure at point A since S_A is approximately constant. In all cases, u_A was found to be less than 1% of the reflected-shock velocity, supporting the $S_A = S_B$ assumption.

Model Results

The reflected-shock model was validated by comparing the predicted temperature (and pressure) rise with the measured values from the CO-emission experiments presented above. Table 3 lists the predicted and measured ΔT_5 at t = 500 μs for a representative range of data from the original Table 1 compilation. Measured incident-shock Mach number, attenuation. and the initial conditions serve as the only input variables. The model compares well with experiment, and the calculated temperature rise is, in general, within 5 K for a wide range of incident-shock attenuation (1.5 - 4.0 %/m) and Mach number (2.2 - 2.6). The few examples where the disagreement is 5 K or more are, however, not surprising and can be attributed to the uncertainty and variation in the attenuation, as seen in Fig. 1, and to the uncertainties in defining a dI/dt from the CO-emission measurements.

Table 3 Comparison between calculated and measured temperature increase at 500 μs after arrival of reflected shock wave.

	T	P	ΔT at 500 μs			T	P	ΔT at 500 μs	
Run	(K)	(atm)	Meas	Model	Run	(K)	(atm)	Meas	Model
862	1450	19.6	38	34	1103	1628	198.8	24	25
875	1275	61.1	22	20	1104	1460	205.3	19	22
884	1379	62.3	26	25	1105	1624	166.4	20	26
885	1641	59.2	38	34	1106	1439	181.3	16	18
887	1489	59.2	31	26	1131	1445	176.7	18	17
888	1783	52.8	39	37	1132	1499	173.8	17	20
890	1815	52.8	35	38	1133	1528	161.4	16	20
891	1522	60.4	26	29	1149	1803	158.7	34	30
892	1521	37.7	25	28	1150	1722	159.8	27	26
897	1335	33.4	23	20	1151	1711	160.8	27	29
915	1424	32.1	31	26	1174	1452	69.2	20	20
931	1410	62.9	22	21	1182	1485	70.7	18	24
932	1598	61.1	29	27	1183	1642	66.8	22	25
933	1493	33.6	28	23	1184	1895	63.3	34	37
938	1546	24.8	31	26	1185	1508	72.6	19	18
1075	1431	67.7	18	21	1191	1581	493.3	19	23
1077	1509	61.7	23	28	1201	1300	166.6	15	15
1096	1611	196.7	18	23	1217	1602	164.0	21	26
1097	1586	63.7	21	20	1221	1771	58.3	40	35
1098	1622	199.1	24	25	1224	1854	162.1	35	31

Because of the good agreement between model and experiment, the theoretical model can be utilized to estimate trends as a function of certain shock tube parameters and test conditions. For example, the effects of test pressure and temperature on the temperature increase were evaluated over a range of P_5 and T_5; predicted attenuation rates using the incident-shock attenuation model [19] were utilized. Figure 6 displays ΔT_5 results at $t = 500$ μs for a pure argon test gas at pressures between 0.1 and 500 atm and temperatures of 1400, 1800, and 2200 K. As pressure increases, the temperature change decreases; the ΔT_5 at 100 atm is nearly 20 K lower than at 1 atm, and there is little difference in the temperature change between 100 and 500 atm. In contrast, the test temperature has a marked effect on the nonideal gas dynamics, where the 500-μs temperature increase can be 30 K higher at 2200 K ($\Delta T = 40$ to 70 K) than at 1400 K ($\Delta T = 5$ to 30 K). In summary, nonideal gas dynamics behind the reflected shock wave are worse at lower pressures and higher temperatures. These trends are due primarily to the increased turbulent boundary layer thickness at lower pressures and higher incident shock wave speeds (i.e., higher test temperatures) [19]. The experimental data in Table 2, the attenuation data in Fig. 1, and the Eqn. 1 attenuation expression support the Fig. 6 trends.

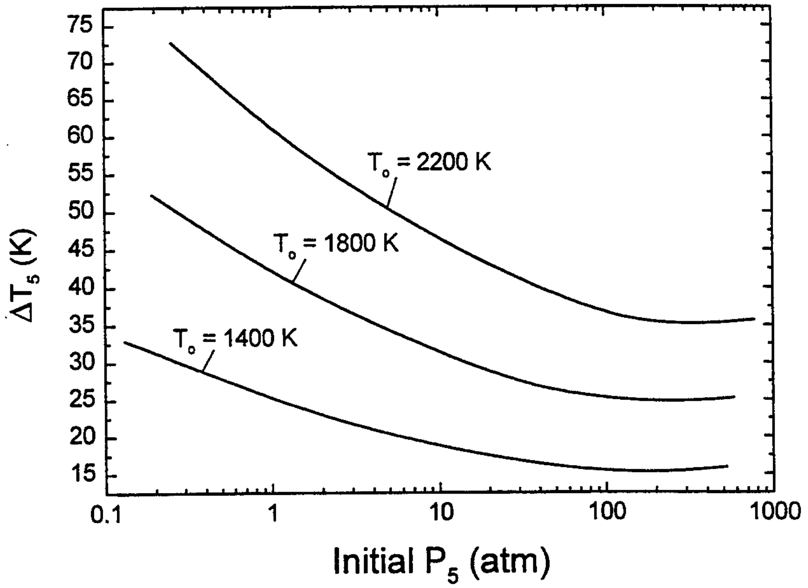

Fig. 6 Effect of pressure and temperature on temperature increase at t = 500 μs behind the reflected shock wave in the HPST (in argon). All values shown were calculated using the reflected-shock model along with the incident-shock model's estimate of the attenuation (including viscous effects only).

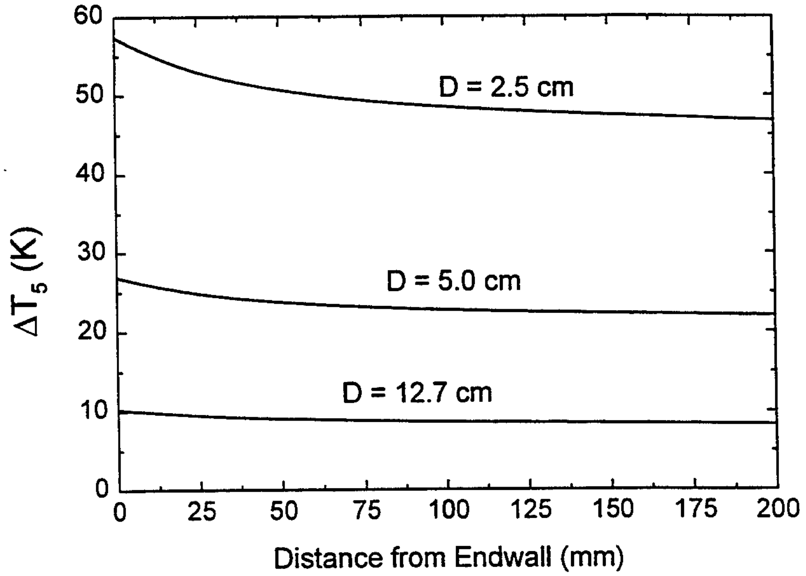

Fig. 7 Effect of shock tube diameter and test section location on the temperature increase behind the reflected shock wave at t = 500 μs. All values were calculated using the reflected-shock model along with the incident-shock model's estimate of the attenuation (including viscous effects only). T_o = 1800 K, P_o = 100 atm, argon.

Although the HPST dimensions are fixed, a useful application of the reflected-shock model is to determine what effects shock tube diameter and test-section location have on nonideal gas dynamics. Presented in Fig. 7 is a comparison of the ΔT_5 at 500 μs for three shock tube diameters: 2.5, 5.0, and 12.7 cm (1, 2, and 5 inches, respectively) over a range of positions relative to the endwall (z = 0 to 200 mm). For the Fig. 7 calculations, the Mach number and P_1 corresponding to a test temperature and pressure of 1800 K and 100 atm, respectively, were used, and a 5-m driven-section length was assumed. The effect of test section location is minimal (< 10 K), while the shock tube diameter has a dramatic impact on the temperature increase. For the 2.5-cm tube, the temperature increase at 20 mm, 500 μs (55 K) is over five times greater than the predicted increase for the larger, 12.7-cm tube (10 K). Hence, as expected, smaller shock tube diameters produce greater nonuniformities because the turbulent boundary layer comprises a greater fraction of the total flow area.

It should be noted that the curves in Figs. 6 and 7 required incident-shock attenuation values; these axial velocity profiles were obtained using the incident-shock attenuation code discussed in Petersen [19] and, thus, include only the effects of friction. The actual 500-μs ΔT's for the HPST would be approximately 5 K higher than those in Figs. 6 and 7 due to additional diaphragm-breakage nonidealities. Nonetheless, the results in Figs. 6 and 7 display the correct trends and are representative of the relative effect that P_5 and T_5 have on the reflected-shock nonuniformities. Since the primary function of the gas dynamic routine described herein is the estimation of reflected-shock nonuniformities for a given attenuation and Mach number, which are measured on every experiment, an *a priori* prediction of the attenuation including both friction and nonideal diaphragm rupture is not needed. The nonideal diaphragm contribution to the attenuation can, of course, be estimated using the friction model and the HPST data in Fig. 1, but the results would only apply to the HPST. The diaphragm effects would differ from shock tube to shock tube while the viscous prediction utilizes a more general procedure.

As demonstrated in the following section, the analytical model can be used to predict the attenuation-induced temperature and pressure increase for any shock tube experiment wherein the axial shock velocity profile is measured. This is the application where the analytical model is most useful because the corrected temperature and pressure can be incorporated into the data reduction process. The effect on shock tube chemistry can then be evaluated.

Discussion

According to the experimental results and the analytical model, the temperature increase behind the reflected shock wave approaches 30 K or more after 500 μs. Such a temperature increase can influence the interpretation of laser absorption- and infrared emission-based species profiles, thus impacting kinetics analysis and data reduction. In this section, sample calculations are utilized to demonstrate the repercussions that nonuniform temperature and pressure have on chemistry experiments. The effects on chemical kinetic calculations are described first, where an indication of the proper analysis techniques and the trends one might expect to see are provided. Species-profile measurements are discussed next, and specific examples employing absorbing molecules of interest in the laboratory are reviewed

Kinetics Calculations

Typically, shock tube chemical kinetics measurements are performed with a test gas composed of a minor constituent mixed with a bath gas such as argon or nitrogen. The large diluent fraction (usually > 97%) serves as the primary third-body, but it also plays the role as a heat sink that minimizes reaction-related temperature changes. In essence, shock tube experiments are designed to provide the conditions of a premixed, constant-temperature and -pressure reactor. However, temperature and pressure changes resulting from a temporally non-uniform post-shock flow field can negate the usual assumption that changes in the reaction temperature and pressure are negligible. The impact of flow non-uniformities on the chemical kinetics must be evaluated and, in certain cases, compensated for.

The effect of increasing temperature and pressure can be determined analytically using Chemkin II [48] by specifying T and P as a function of time *a priori*. This option of Chemkin is in lieu of using the constant-h,P or constant-u,V options, and, of course, assumes that the temperature and pressure increase due to reaction is negligible. To demonstrate, a stoichiometric mixture of 1000 ppm H_2, 500 ppm O_2, balance argon was utilized in the calculations, and the dP/dt and dT/dt values were obtained via the incident- and reflected-shock models. An initial reflected-shock pressure of 65 atm was assumed, and two temperatures were selected (1550 and 1350 K), representing fast and slow chemistry. The detailed kinetics mechanism was taken from the H_2-O_2 subset of the GRI-Mech 1.2 mechanism [49]. Since hydroxyl-radical formation and depletion give a good indication of ignition time and peak mole fraction, OH mole fraction was utilized as the primary Chemkin output.

Figure 8 presents the results of the kinetics model assuming 1) a constant reaction temperature and pressure, and 2) a pressure and temperature increase predicted using the analytical reflected-shock model. The 1550-K results are shown in Fig. 8a, corresponding to $d(T/T_o)/dt = 27.6\ s^{-1}$ and $d(P/P_o)/dt = 69.6\ s^{-1}$ ($\approx$ 3 %/m incident-shock-speed attenuation). At this higher temperature, the kinetics are fast and reaction occurs shortly after 50 μs, evident by the sharp rise in OH. The attenuation-induced temperature increase at the time of reaction is less than 3 K, so the difference between the attenuation-corrected case and the constant-temperature one is insignificant. Key features such as ignition delay time and peak OH mole fraction would be well within experimental error for this 1550-K case.

Discrepancies, however, become more pronounced at 1350 K, where the ignition delay time is longer. Figure 8b presents the 1350-K comparison, corresponding to a $d(T/T_o)/dt$ and a $d(P/P_o)/dt$ of 25.5 and 64.2 s^{-1}, respectively. The ignition time for the constant-temperature case is near 400 μs, in contrast to the attenuation-corrected result which has a reaction time that is 35 μs shorter (9% error). In addition, the peak OH mole fraction is greater when nonideal effects are included, primarily because the temperature increases by 15 K prior to ignition (for an average temperature of 1358 K). Similarly, the radical-decay characteristics are different at longer times.

The results displayed in Fig. 8 are representative of the effects nonuniform reflected-shock conditions have on chemical kinetics. In summary, reactions that occur within the first few hundred microseconds are not impacted as much as reactions that extend to longer times. Therefore, the effects of the temperature increase can be minimized via proper experimental design by choosing mixtures and conditions wherein the important kinetics occur at early times.

Alternatively, the temperature increase can be inferred from the reflected-shock model, described herein (using the measured attenuation and M_s); using this temperature change, the kinetics analysis of the experimental data can be corrected for the nonuniform conditions.

Unfortunately, the specified-(T, P) option in Chemkin and the prediction of energy release due to reaction are mutually exclusive. Unless a model exists that integrates the kinetics with the energy changes behind the reflected shock wave, gas dynamic corrections should only be made when the ΔT due to attenuation overshadows the ΔT expected from exothermic reactions. Such a model would simply have to combine the energy release due to the kinetics with the time-dependent gas dynamics.

Species Profile Measurements

While the nonuniform temperature and pressure behind the reflected shock wave impact the chemical kinetics, they can also impact the data reduction process. In cw laser absorption measurements, the absorption cross section of the absorbing molecule is often temperature-dependent, and pressure broadening and shift often affect the frequency-dependent lineshape function. Therefore, changes in the temperature and pressure during the course of an experiment can affect the interpretation of absorption data via the absorption coefficient and the pressure term in Beer's Law. To gauge the magnitude of the effect, two common shock tube absorbing molecules with different temperature and pressure sensitivities are discussed: OH and CH_3. In infrared-emission measurements, the data are sensitive to temperature changes, as seen in the CO measurements above and briefly described below.

OH Absorption. The OH molecule is an important chain-branching radical in most combustion systems, particularly in oxidative environments wherein hydrogen and/or hydrocarbons are the fuel. Since its development by Rea et al. [50,51], cw ring-dye laser absorption monitoring of OH has been a primary shock tube diagnostic in low-pressure shock tubes and, more recently, in the High Pressure Shock Tube [52]. As summarized by Rea et al., the OH absorption coefficient depends on the collision width and collision shift, both of which exhibit temperature and pressure dependence. In Davidson et al. [52], the broadening and shift of the OH A-X (0,0) bandhead near 306 nm was characterized at high pressure and temperature (60 atm, 1735 K) in argon. The 306-nm laser light was accessed via a cw ring-dye laser operating at 612 nm, frequency-doubled using an intra-cavity AD*A crystal. The measured collision width, $\Delta\nu_{width}$, at elevated pressure was found to vary with temperature and pressure as follows:

$$\Delta\nu_{width} \propto PT^{-0.75} \qquad (12)$$

The shift, $\Delta\nu_{shift}$, is similarly dependent on T and P:

$$\Delta\nu_{shift} \propto -PT^{-0.45} \qquad (13)$$

Changes in temperature and pressure during the course of an experiment can affect the spectral absorption coefficient, and hence the OH mole fraction, via the T and P dependencies in Eqns. 12 and 13.

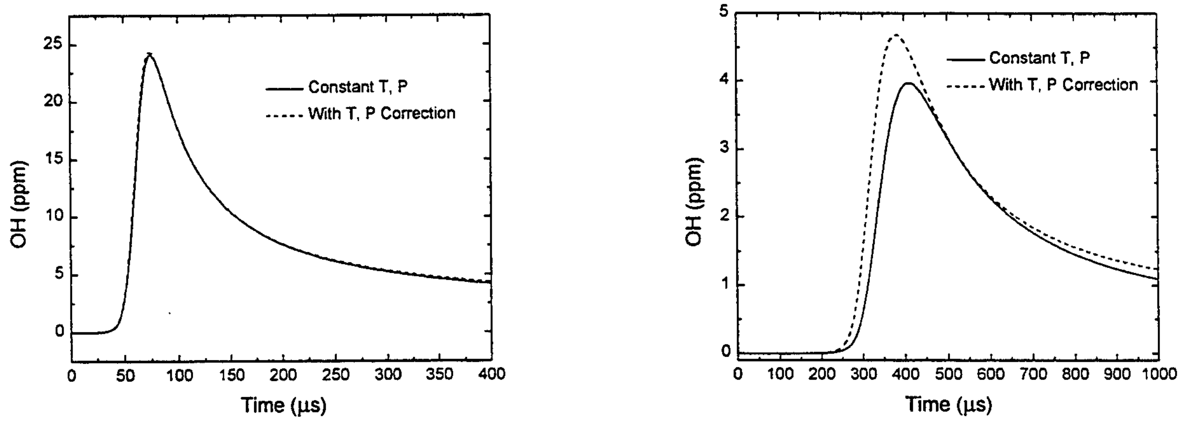

(a) 1550, 65 atm (fast kinetics)

(b) 1350 K, 65 atm (slow kinetics)

Fig. 8 Predicted OH mole fraction in the HPST assuming: 1) constant T_o and P_o, and 2) T_o and P_o as predicted by reflected-shock model. 1000 ppm H_2, 500 ppm O_2, balance argon.

Using typical HPST values for ΔT_5 and ΔP_5, and a specified mixture with known kinetics, the change in absorption coefficient and, hence, the change in the percent absorption of the laser light can be predicted analytically. (This situation is simply the inverse of what normally occurs during an experiment, where the percent absorption is measured and the mole fraction is inferred from Beer's Law.) For example, assuming OH is produced in a mixture of 0.1% H_2, 0.05% O_2 in argon, shock heated initially to 65 atm and 1350 K, the temperature and pressure after 1 ms would increase to 1384 K and 69.2 atm ($\Delta T = 34$ K, $\Delta P = 4.2$ atm).

A comparison of the OH A-X (0,0) band at t = 0 and t = 1ms is provided in Fig. 9, calculated per Davidson et al. [52]. There is little difference between the two spectra at the key frequency of 32630 cm^{-1}. The corresponding OH profiles, calculated using Chemkin, the GRI-Mech 1.2 mechanism, and Beer's Law, are presented in Fig. 10. The difference between the t=0 and t=1 ms profiles is less than 0.1%, which is well within the accuracy of the laser absorption technique in the High Pressure Shock Tube.

The results of Fig. 10 indicate that the attenuation effects should not have a large impact on the interpretation of OH profiles obtained using laser absorption near 306 nm. The actual k_ν at 32630 cm^{-1} varies only from 20.0 $atm^{-1}cm^{-1}$ at time zero to 19.2 after 1 ms for the conditions of Fig. 10, and the effects of the decreasing absorption coefficient are offset by the increasing pressure in the Beer's Law exponent. This outcome is coupled with the fact that most measurements should be complete long before 1 ms is reached, preferably within the first few hundred microseconds as discussed above. Therefore, for the majority of HPST experiments, a single OH absorption coefficient (defined at T_o and P_o) and the initial pressure can be utilized in the Beer's Law conversion of raw data from percent absorption to mole fraction. Of course, this assumption can be easily verified for each set of experiments using the procedure outlined above.

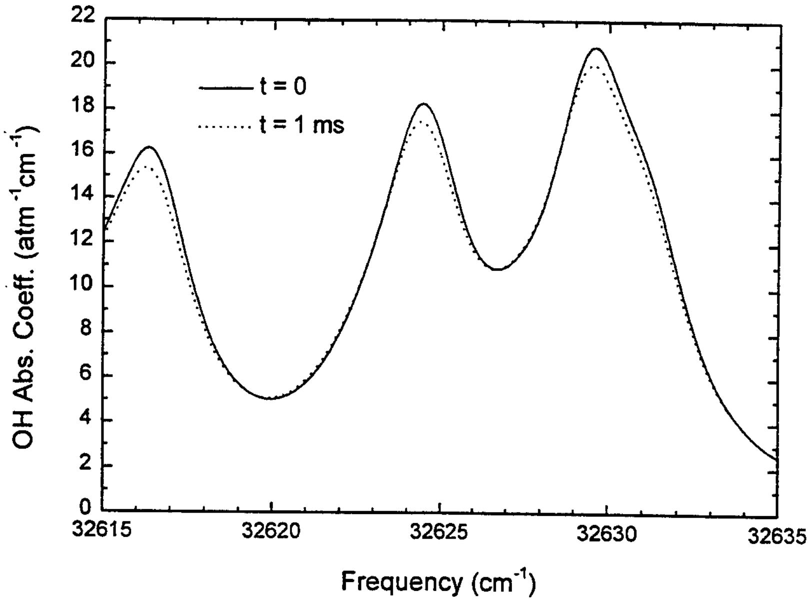

Fig. 9 OH absorption coefficient for A-X (0,0) 306-nm Bandhead at t = 0 and t = 1 ms after passage of the reflected shock wave (including the temperature and pressure increase predicted by the reflected-shock gas dynamic model). T_o = 1350 K, P_o = 65 atm; T (1 ms) = 1384 K, P(1 ms) = 69.2 atm. Calculated per Davidson et al. [52].

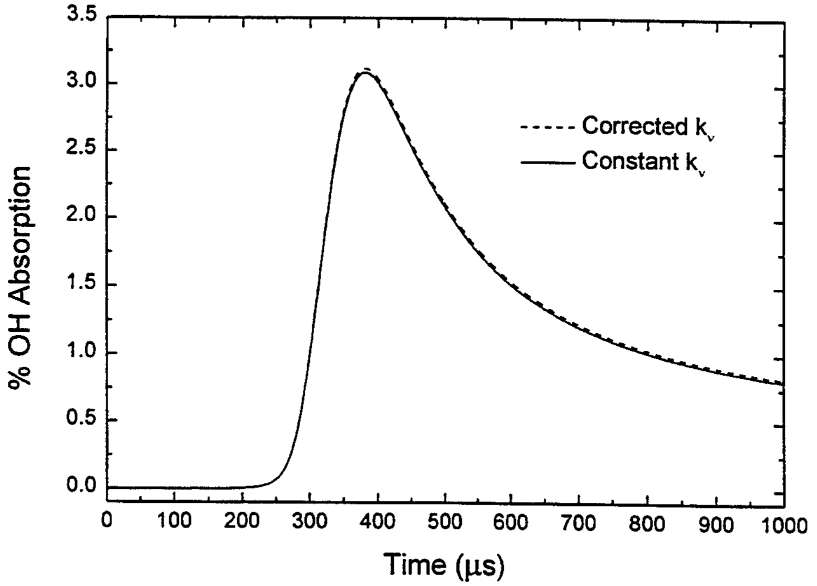

Fig. 10 OH absorption profiles calculated assuming: 1) a constant absorption coefficient and, 2) one which changes per the calculated T_o and P_o increase. Initial conditions are 1350 K and 65 atm, 1000 ppm H_2 + 500 ppm O_2, balance argon; T(1 ms) = 1384 K, P(1 ms) = 69.2 atm.

Methyl Absorption. Another key combustion radical and shock tube diagnostic is CH_3. The primary wavelength of interest is 216.615 nm, corresponding to the Hertzberg β_1 band at high temperature [53]. Assuming the pressure dependence at HPST conditions is small, the absorption coefficient of methyl at 216.615 nm given by Davidson et al. [53] is assumed herein to be valid at elevated pressures:

$$k_{\lambda_{CH_3}} = (562{,}400 / T)\exp(-T / 1087) \tag{14}$$

where k_λ is the spectral absorption coefficient (arm^{-1}cm^{-1}) and T is the temperature in K. Equation 14 was used to estimate the effect of reflected-shock nonuniformities on the interpretation of CH_3 absorption data in the HPST.

The formation and depletion of methyl was calculated using GRI-Mech 1.2 to model the decomposition of 100-ppm CH_4 in argon, and the initial conditions downstream of the reflected shock wave were assumed to be 1800 K and 100 atm. A temperature increase of $d(T/T_0)/dt = 30.5\ s^{-1}$ and a pressure increase of $d(P/P_0)/dt = 70\ s^{-1}$ were calculated for these specific conditions; this corresponds to a temperature of 1854 K and a pressure of 107.7 atm 1 ms after shock arrival ($\Delta T = 54$ K, $\Delta P = 7.7$ atm). The absorption coefficient calculated with Eqn. 14 is 59.6 atm^{-1}cm^{-1} at t = 0 and decreases to 55.1 atm^{-1}cm^{-1} after one millisecond. Figure 11 shows the calculated CH_3 absorption assuming: 1) a constant T and P equal to the initial values, and 2) an increasing T and P per the calculated nonuniformity. Both OH profiles are virtually identical, as seen in Fig. 10, i.e., the increasing pressure offsets the decreasing absorption coefficient.

The results of Fig. 11 indicate HPST attenuation does not have a significant impact on conversions between CH_3 absorption profiles and CH_3 mole fraction profiles, and a single k_ν defined at the initial T_5 and P_5 should be adequate for laser absorption measurements near 216 nm.

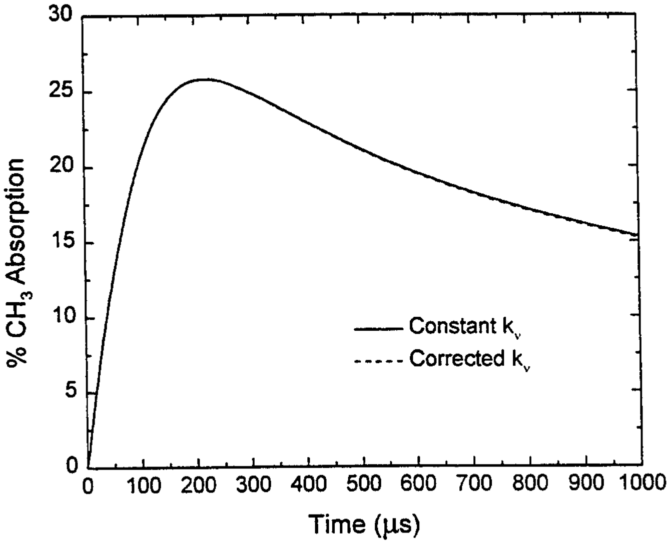

Fig. 11 Calculated CH_3 absorption profiles for: 1) a constant absorption coefficient and, 2) one which changes per the calculated T_5 and P_5 increase. Initial conditions are 1800 K and 100 atm, 100 ppm CH_4, balance argon; T(1 ms) = 1854 K, P(1 ms) = 107.7 atm.

Infrared Emission. Unlike the interpretation of the absorption data, the increasing temperature and pressure behind the reflected shock wave can significantly affect the IR emission data. According to harmonic oscillator theory, the measured infrared emission from a vibrating molecule depends on the temperature and pressure according to [41]

$$I \propto \frac{P / T}{\exp(\theta_v / T) - 1} \tag{15}$$

Hence, the emission signal is sensitive to changes in the test temperature and pressure on the order of the nonideal effects behind the reflected shock wave. Figure 12 presents two X_{CO} plots as inferred from a CO-emission trace (via Eqn. 2) for a 0.08% CO/0.15% H_2/99.77% Ar mixture with an initial T_5 and P_5 of 1803 K and 159 atm. The top plot is uncorrected for the changing T_5 and P_5, while the lower curve includes the appropriate T_5 and P_5 changes using Eqns. 4, 5, and 6. The interpretation error for the uncompensated CO-emission trace would be appreciable, but adjustment of the signal to account for the increasing T and P brings the inferred CO mole fraction to a straight line, as expected since the CO does not decompose at 1803 K. Similar compensation should also be done when analyzing IR emission data from other molecules such as CH_4 and N_2O. When the mole fraction of the emitting species is not known, the measured dP/dt can be used to infer the correct I and T correction via Eqns. 4, 5, and 6.

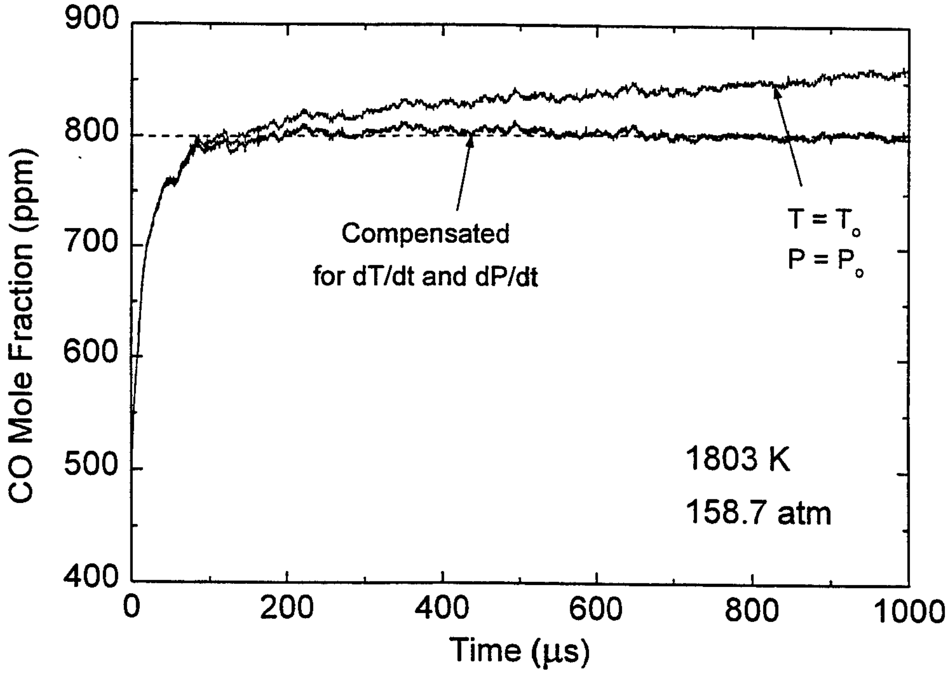

Fig. 12 CO mole fraction inferred from a measurement of CO emission near 4.7 μm; 0.8% CO + 0.15% H_2 + Ar; 1803 K, 159 atm. T_5 and P_5 after 1 ms are 1871 K and 174 atm, respectively. The upper curve is uncompensated and therefore includes the effects of the changing T_5 and P_5. By accounting for ΔT_5 and ΔP_5, the inferred mole fraction is constant in the lower curve, as expected.

Summary

Experiments and calculations related to the measurement and prediction of nonideal gas dynamic effects in the Stanford High Pressure Shock Tube were presented. Because of its importance in chemical kinetic measurements, changes in the test temperature behind the reflected shock wave were highlighted. The change in temperature at a location 2 cm from the endwall was characterized experimentally using an IR-emission technique. Emission from trace levels of CO was used to infer dT/dt, assuming an isentropic relationship between the test temperature and pressure, over a representative range of conditions in argon (20 - 530 atm, 1240 - 1900 K). Typically, the temperature increased 3-8 K after 100 μs and 15-40 K after 500 μs, corresponding to near-linear (normalized) temperature and pressure slopes. Separate experiments with a shielded pressure transducer minimized heat transfer effects to the gauge, leading to dP/dt measurements that support the isentropic relationship between pressure and temperature. The change in test temperature can thus be inferred from routine measurements of dP/dt using a shielded pressure transducer since the relationship between T and P is nearly isentropic.

An analytical model was presented that reproduces the nonideal gas dynamics behind the reflected shock wave. The nonuniform conditions upstream of the reflected shock wave were defined using the incident-shock attenuation theory of Petersen [19] and Mirels [3,4], and the perturbations between the reflected shock wave and the endwall were assumed to propagate along right- and left-running characteristics. The results of the model agree well with experiment; the calculated post-shock ΔT's are, in general, within a few K of the temperature increases obtained with the CO-emission technique. In general, the nonideal effects are greatest at lower pressures and higher temperatures. Since the temperature increase cannot realistically be measured during every experiment, the reflected-shock model can be used, with confidence, in predicting the nonideal conditions behind the reflected shock wave.

In the final section, the effects of increasing test temperature and pressure on chemistry measurements in the HPST were evaluated. Calculations using a chemical kinetics model of H_2-O_2 combustion demonstrated that a positive dT/dt influences the chemistry to a greater extent when the reaction times are longer than approximately 300 - 500 μs. Therefore, proper experimental design should focus on reactions that occur within the first few hundred microseconds. If nonideal effects cannot be avoided, the accompanying kinetics analysis using a detailed mechanism can be performed for a specified dT/dt and dP/dt prior to comparison with the nonideal data. Separate calculations indicate the reduction of laser absorption data for at least two key species, OH (306 nm) and CH_3 (216 nm), requires little, if any, correction for the changing absorption coefficient since the impact on the mole fraction inferred from Beer's Law is minimal. In contrast, species profiles obtained via ir emission are much more sensitive to changes in T and P, so the data should be compensated accordingly.

Acknowledgements

The Department of Energy, the Office of Naval Research, and the Army Research Office supported this work. The authors wish to thank Dr. David Davidson and Ronald Bates for assistance on the shock tube experiments.

References

1. Bowman, C. T. and Hanson, R. K., "Shock Tube Measurements of Rate Coefficients of Elementary Gas Reactions," *J. Physical Chemistry*, Vol. 83, No. 6, 1979, pp. 757-763.

2. Röhrig, M., Petersen, E. L., Davidson, D. F., and Hanson, R. K., "A Shock Tube Study of the Pyrolysis of NO_2," *International Journal of Chemical Kinetics*, Vol. 29, 1997, pp. 483-493.

3. Mirels, H., "Test Time in Low-Pressure Shock Tubes," *Physics of Fluids*, Vol. 6, No. 9, 1963, pp. 1201-1214.

4. Mirels, H., "Shock Tube Test Time Limitation Due to Turbulent-Wall Boundary Layer," *AIAA Journal*, Vol. 2, No. 1, 1964, pp. 84-93.

5. Warshay, M., "Effects of Boundary Layer Buildup in Shock Tubes upon Chemical Rate Measurements," NASA TN D-4795, Sept. 1968.

6. Belford, R. L. and Strehlow, R. A., "Shock Tube Technique in Chemical Kinetics," *Annual Review of Physical Chemistry*, Vol. 20, 1969, pp. 247-272.

7. Belles, F. E. and Brabbs, T. A., "Experimental Verification of Effects of Turbulent Boundary Layers on Chemical-Kinetic Measurements in a Shock Tube," *Thirteenth Symposium (International) on Combustion*, The Combustion Institute, Pittsburgh, 1971, pp. 165-175.

8. Brabbs, T. A. and Belles, F. E., "Experimental Study of Effects of Laminar Boundary Layers on Chemical-Kinetic Measurements in a Shock Tube," *Shock Tube Research, Proceedings of the Eighth International Shock Tube Symposium*, Chapman and Hall, London, 1972, p. 24.

9. Bertin, J. J., Ehrhardt, E. S., Gardiner, W. C. Jr., and Tanzawa, T., "Study of Improved Models for Laminar Shock Tube Boundary Layers in Chemically Reactive Test Gas," *Modern Developments in Shock Tube Research, Proceedings of the Tenth International Shock Tube Symposium*, Shock Tube Research Society, Japan, 1975, pp. 595-604.

10. Fujii, N., Koshi, M., Ando, H., and Asaba, T., "Evaluation of Boundary-Layer Effects in Shock-Tube Studies of Chemical Kinetics," *International Journal of Chemical Kinetics*, Vol. 11, 1979, pp. 285-304.

11. Koshi, M. and Asaba, T., "Shock-Tube Study of Thermal Decomposition of Nitric Oxide between 2700 and 3500 K," *International Journal of Chemical Kinetics*, Vol. 11, 1979, pp. 305-315.

12. Strehlow, R. A. and Cohen, A., "Comment on Reflected Shock Wave Studies," *Journal of Chemical Physics*, Vol. 28, 1958, pp. 983-985.

13. Skinner, G. B., "Limitations of the Reflected Shock Technique for Studying Fast Chemical Reaction," *Journal of Chemical Physics*, Vol. 31, 1959, pp. 268-269.

14. Brabbs, T. A., Zlatarich, S. A., and Belles, F. E., "Limitations of the Reflected-Shock Technique for Studying Fast Chemical Reactions," *Journal of Chemical Physics*, Vol. 33, 1960, pp. 307-308.

15. Strehlow, R. A. and Case, C. T., "Limitations of the Reflected Shock Technique for Studying Fast Chemical Reactions," *Journal of Chemical Physics*, Vol. 35, 1961, pp. 1506-1507.

16. Johnson, C. D. and Britton, D., "Shock Waves in Chemical Kinetics: The Use of Reflected Shock Waves," *Journal of Chemical Physics*, Vol. 38, 1963, pp. 1455-1462.

17. Fishburne, E. S., Bergbauer, D. M., and Edse, R., "Chemical Kinetics and the Reflected Shock Wave," *Physics of Fluids*, Vol. 7, 1964, pp. 1391-1392.

18. Presley, L. L. and Hanson, R. K., "Numerical Solutions of Reflected Shock-Wave Flowfields with Nonequilibrium Chemical Reactions," *AIAA Journal*, Vol. 7, No. 12, 1969, pp. 2267-2273.

19. Petersen, E. L., "A Shock Tube and Diagnostics for Chemistry Measurements at Elevated Pressures with Application to Methane Ignition," Ph.D. Thesis, Department of Mechanical Engineering, Stanford University, March 1998.

20. Rothkopf, E. M. and Low, W., "Diaphragm Opening Process in Shock Tubes," *Physics of Fluids*, Vol. 17, No. 6, 1974, pp. 1169-1173.

21. White, D. R., "Influence of Diaphragm Opening Time on Shock-Tube Flows," *Journal of Fluid Mechanics*, Vol. 4, 1958, pp. 585-599.

22. Simpson, C. J. S. M., Chandler, T. R. D., and Bridgman, K. B., "Effect on Shock Trajectory of the Opening Time of Diaphragms in a Shock Tube," *Physics of Fluids*, Vol. 10, No. 9, 1967, pp. 1894-1896.

23. Tajima, K., Outa, E., and Nakada, G., "Some Investigations of Shock Tube Flow," *Bulletin of the JSME*, Vol. 11, No. 43, 1968, pp. 116-124.

24. Ikui, T. and Matsuo, K., "Investigations of the Aerodynamic Characteristics of the Shock Tubes (Part 1, The Effects of the Tube Diameter on the Tube Performance)," *Bulletin of the JSME*, Vol. 12, No. 52, 1969, pp. 774-782.

25. Ikui, T, Matsuo, K., and Nagai, M., "Investigations of the Aerodynamic Characteristics of the Shock Tubes (Part 2, On the Formation of Shock Waves)," *Bulletin of the JSME*, Vol. 12, No. 52, 1969, pp. 783-792.

26. Outa, E., Tajima, K., and Hayakawa, K., "Shock Tube Flow Influenced by Diaphragm Opening (Two-Dimensional Flow Near the Diaphragm)," *Modern Developments in Shock Tube Research, Proceedings of the Tenth International Shock Tube Symposium*, 1975, pp. 312-319.

27. Rothkopf, E. M. and Low, W., "Shock Formation Distance in a Pressure Driven Shock Tube," *Physics of Fluids*, Vol. 19, No. 12, 1976, pp. 1885-1888.

28. Gaydon, A. G. and Hurle, I. R., *The Shock Tube in High-Temperature Chemical Physics*, Reinhold, New York, 1963.

29. Parkinson, W. H. and Nicholls, R. W., "Spectroscopic Temperature Measurements in a Shock Tube Using CN as a Thermometric Molecule," *Canadian Journal of Physics*, Vol. 38, 1960, pp. 715-719.

30. Napier, D. H., Nettleton, M., Simonson, J. R., and Thackeray, D. P. C., "Temperature Measurement in a Chemical Shock Tube by Sodium-Line Reversal and C2 Reversal Methods," *AIAA Journal*, Vol. 2, No. 9, 1964, pp. 1136-1138.

31. Tsuchiya, S. and Kuratani, K., "Temperature Measurement of Argon Gas behind Reflected Shock Wave," *Journal of Chemical Physics*, Vol. 42, 1965, pp. 2986-2987.

32. Rea, E. C. Jr., Salimian, S., and Hanson, R. K., "Rapid-Tuning Frequency-Doubled Ring Dye Laser for High Resolution Absorption Spectroscopy in Shock-Heated Gases," *Applied Optics*, Vol. 23, 1984, pp. 1691-1694.

33. Chang, A. Y., Rea, E. C. Jr., and Hanson, R. K., "Temperature Measurements in Shock Tubes Using a Laser-Based Absorption Technique," *Applied Optics*, Vol. 26, 1987, pp. 885-891.

34. Lapworth, K. C., Allnutt, L. A., and Pendlebury, J. R., "Temperature Measurements in Shock-Heated Carbon Monoxide by an Infrared Technique," *Journal of Physics D: Applied Physics*, Vol. 4, 1971, pp. 759-768.

35. Guinee, M. J., Hewitt, F. A., Fussey, D. F., Milton, B. E., and Palmer, T. F., "The Formation of Oxides of Nitrogen from $CH_4/O_2/N_2$ Mixtures," *Shock Tubes and Waves, Proceedings of the 12th International Symposium on Shock Tubes and Waves*, The Magnes Press, Jerusalem, 1980, pp. 495-502.

36. Just, Th. and Schmalz, F., "Measurements of Ignition Delays of Hydrogen-Air Mixtures under Simulated Conditions of Supersonic Combustion Chambers," AGARD Conference Proceedings No. 34, Sept. 1968, p. 19.

37. Flower, W. L., "Experimental Study of Nitric Oxide-Hydrogen Reaction Kinetics," Ph.D. Thesis, Department of Mechanical Engineering, Stanford University, March 1976.

38. Hayashi, A. K. and Goto, M., "Low Temerature Ignition of N-Butane in a Tailored Condition behind a Reflected Shock Wave," *Current Topics in Shock Waves, 17th International Symposium on Shock Waves and Shock Tubes*, AIP, New York, 1990, pp. 713-718.

39. Ciezki, H. and Adomeit, G., "Shock-Tube Investigation of the Ignition Delay on n-Heptane/Air-Mixtures in a High Pressure Shock Tube under Conditions Relevant to Diesel-Engine Combustion," *Current Topics in Shock Waves, 17th International Symposium on Shock Waves and Shock Tubes*, AIP, New York, 1990, pp. 707-712.

40. Davidson, D. F., Bates, R. W., Petersen, E. L., and Hanson, R. K., "Shock Tube Measurements of the Equation of State of Argon," *International Journal of Thermophysics*, in press, 1999; also, presented at the 13th Symposium on Thermophysical Properties, Boulder CO, June 22-27, 1997.

41. Vincenti, W. G. and Kruger, C. H. Jr., *Introduction to Physical Gas Dynamics*, Krieger, Malabar, 1965.

42. Rudinger, G., "Effect of Boundary-Layer Growth in a Shock Tube on Shock Reflection from a Closed End," *Physics of Fluids*, Vol. 4, 1961, pp. 1463-1473.

43. Hanson, R. K. and Baganoff, D., "Reflection of a Shock Wave into a Density Gradient," *AIAA Journal*, Vol. 8, No. 4, 1970, pp. 805-807.

44. Hanson, R. K., "Shock Wave Reflexion in a Relaxing Gas," *J. Fluid Mechanics*, Vol. 45, 1971, pp. 721-746.

45. Michael, J. V. and Sutherland, J. W., "The Thermodynamic State of the Hot Test Gas behind Reflected Shock Waves: Implication to Chemical Kinetics," *International Journal of Chemical Kinetics*," Vol. 18, 1986, pp. 409-436.

46. Michael, J. V. and Fisher, J. R., "Corrections for Non-Ideal Effects in Reflected Shock Waves at Low Mach Numbers," *Current Topics in Shock Waves, 17th International Symposium on Shock Waves & Shock Tubes*, Kim, Y. W. (ed.), AIP, New York, 1990, pp. 210-215.

47. Rudinger, G., *Nonsteady Duct Flow: Wave-Diagram Analysis*, Dover, New York, 1969.

48. Kee, R. J., Rupley, F. M., and Miller, J. A., "Chemkin-II: A Fortran Chemical Kinetics Package for the Analysis of Gas-Phase Chemical Kinetics," Sandia National Laboratories Report, SAND89-8009, 1989.

49. Frenklach, M., Wang, H., Goldenberg, M., Smith, G. P., Golden, D. M., Bowman, C. T., Hanson, R. K., Gardiner, W. C., and Lissianski, V., "GRI-Mech--An optimized Detailed Reaction Mechanism for Methane Combustion," GRI Topical Report No. GRI-95/0058, 1995.

50. Rea, E. C., Salimian, S., and Hanson, R. K., "Rapid-Tuning Frequency-Doubled Ring Dye Laser for High Resolution Absorption Spectroscopy in Shock-Heated Gases," *Applied Optics*, Vol. 23, 1984, pp. 1691-1694.

51. Rea, E. C. Jr., "Rapid-Tuning Laser Wavelength Modulation Spectroscopy with Applications in Combustion Diagnostics and OH Line Shape Studies," Ph.D. Thesis, Department of Mechanical Engineering, Stanford University, March 1991.

52. Davidson, D. F., Roehrig, M., Petersen, E. L., DiRosa, M. D., and Hanson, R. K., "Measurements of the OH A-X (0,0) 306 nm Absorption Bandhead at 60 atm and 1735 K," *Journal of Quantitative Spectroscopy and Radiative Transfer*, Vol. 55, 1996, pp. 755-762.

53. Davidson, D. F., Chang, A. Y., DiRosa, M. D., and Hanson, R. K., "A CW Laser Absorption Diagnostic for Methyl Radicals," *Journal of Quantitative Spectroscopy and Radiative Transfer*, Vol. 49, 1993, pp. 559-571.